ADVANCED ELECTRONIC MATERIALS
www.advelectronicmat.de

Mechanical Nanoscale Polarization Control in Ferroelectric PVDF-TrFE Films

*Robert Roth, Martin M. Koch, A. Diana Rata, and Kathrin Dörr**

Ferroelectric polymer films offer strong advantages like mechanical flexibility, biocompatibility, optical transparency, and low-cost processing. However, their dielectric or piezoelectric performance is often inferior to that of oxide ferroelectric materials. Key to the dielectric or piezoelectric performance of semicrystalline polymers is the enhancement of electric dipolar order that is naturally lower than in crystalline ferroelectrics. Here, reorientation and alignment of the electric polarization in thin films by the mechanical effect of a scanning unbiased force microscopy tip is demonstrated as a versatile tool for nanoscale domain writing. Thin films (50–150 nm) of PVDF-TrFE (78:22) on graphite are prepared with dense (1̲10)-oriented β-phase lamellae randomly oriented in the film plane. The in-plane polarization can be poled "mechanically" along any deliberately chosen direction in the film plane after vertical electric poling. Domain patterns with resolution down to ≈50 nm are written with four (out of six possible) local polarization orientations. Written domains show excellent long-time stability. The surface roughening from the mechanical treatment is moderate (rms roughness of 2–3 nm). A ferroelastic origin of the mechanical polarization switching is discussed. Finally, suggestions are made how to utilize the domain patterns in thin film devices.

1. Introduction

Among the ferroelectric materials of technological interest, polymers like PVDF-TrFE (poly(vinylidenedifluoride-co-trifluoroethylene)) offer the advantages of low-cost processing, non-toxicity, mechanical flexibility, biocompatibility, and optical transparency. This has triggered an enormous growth of activities in applied research on ferroelectric polymer films during recent years. Major research fields address piezoelectric sensors and energy harvesting devices,[1–6] ferroelectric field-effect transistors, and data storage devices[7–12] as well as photoelectronic applications,[8] to name just a few. A crucial limitation of ferroelectric polymers, however, is the considerable level of disorder of electric dipoles that is present practically in all bulk and thin-film samples. Partially, disorder is a consequence of the semicrystalline microstructure of polymers. It severely reduces the averaged electric or mechanical responses to an electric field. This limits the piezoelectric and dielectric performance parameters of actuators, sensors, energy storage, and further functional devices. Therefore, approaches for improving the electric dipolar order in ferroelectric polymer materials are highly desirable.

Thin films of PVDF-TrFE with thicknesses from a few nanometers up to several 100 nm are components in various functional devices. Their microstructure commonly comprises of crystalline lamellae surrounded by amorphous phase. Lamellae are shaped "sheet-like", i.e., they feature one short and two long extensions.[13] The dimensions and arrangements of polymer lamellae are controllable by the preparation conditions of thin films.[13–18] The dipole order without an applied electric field is constrained by the allowed polarization directions in the crystalline lattice.

Electric reorientation of the polarization in PVDF-TrFE requires rather large electric fields.[19,20] In thin films, local application of an electric field by a nanoscale force microscopy tip has been intensely studied for electric poling and domain writing (e.g.,[9,12,17,20–24]). All components of the electric polarization, the vertical and two orthogonal ones in the film plane, can be detected using vertical and lateral piezoresponse force microscopy (PFM).[24] The vertical field component at the microscopy tip can be used to align the vertical component of the electrical polarization. The lateral component of the polarization, i. e., the polarization in the film plane, is mostly unchanged in these studies. It is known from studies on oxide ferroelectrics that the in-plane component of the electric tip field can be used for alignment of the in-plane polarization, exploiting the so-called tip-trailing field.[25] This also works for PVDF-TrFE films, but it needs very large tip fields causing strong stray-field effects and possibly sample damage. An example is shown in Figure S7 (Supplementary Information).

Mechanical treatments of thin films by force microscopy tip have been previously suggested in order to enhance the crystalline order.[22,26,27] Choi et al. reported a strong increase of the vertical and lateral piezoelectric responses in PVDF-TrFE films after scanning areas at the film surface with a mechanical tip force of 600–1400 nN applied with a tip of ≈30 nm radius.[22] They attributed the improved piezoelectric performance to a

R. Roth, M. M. Koch, A. D. Rata, K. Dörr
Institute of Physics
Martin Luther University Halle-Wittenberg
06099 Halle, Germany
E-mail: kathrin.doerr@physik.uni-halle.de

The ORCID identification number(s) for the author(s) of this article can be found under https://doi.org/10.1002/aelm.202101416.

DOI: 10.1002/aelm.202101416

tip-induced crystalline reconstruction including an improved alignment of polymer lamellae. This work as well as reports on flexoelectric polarization switching of PVDF-TrFE films[10,28] motivated our previous investigation.[29] Using a smaller tip force of 100–300 nN and tips of ≈35 nm radius, efficient alignment of the in-plane polarization had been demonstrated in micron-sized domains without significant surface roughening. The alignment of the in-plane polarization multiplied the lateral piezoresponse (depending on the as-grown state, by more than a factor of four) in comparison to the as-prepared films. In contrast to the approach of Choi et al.,[22] structural reconstruction was limited to a surface layer of few nm: the original lamellar microstructure was detectable underneath this surface layer with secondary electrons in scanning electron microscopy.[29]

The origin of the alignment of the in-plane polarization present after scanning an area with electrically unbiased tip (loaded with a medium force of ≤300 nN) has remained open in that previous work[29] and will be addressed here. Further, we identify a pathway to set the electrical polarization in PVDF-TrFE films in four distinct local orientations using electrical poling and mechanical scans with a force microscopy tip. Complex nanoscale domain patterns with a resolution of ≈50 nm have been defined. The physical mechanism underlying the polarization alignment by a tip-induced force is argued to be of ferroelastic nature.

2. Results and Discussion

2.1. Crystalline Phase, Lattice Orientation, and Microstructure of Samples

In order to check the structural phase of our thin film samples (ferroelectric β-phase, presence of impurity phases), X-ray diffraction θ–2θ scans of films on substrates and of bare substrates have been taken. The substrate (HOPG glued onto Si) has a broad background signal which was subtracted to obtain the film data. **Figure 1** shows an example of a film diffraction pattern; the error of θ has been corrected using the graphite peak as a reference. Figure 1 reveals a β-phase (200)/($\underline{1}$10) peak at the fitted position of 20.06° that is slightly above the expected value of 19.96° for unstrained films. This indicates a shortening of the vertical lattice parameter. No traces of other phases like the non-ferroelectric α-phase expected near 17.7° (marked in Figure 1) have been found. This excludes the presence of other phases within the detection limit of the X-ray diffraction measurement that is estimated as ≈5%. With the reported film preparation procedure, we did not detect impurity phases using such x-ray diffraction scans.

The PVDF-TrFE films on graphite are found to be (100)/($\underline{1}$10) oriented along the film normal direction (Figures S2 and S3, Supporting Information); both orientations cannot be separated due to the peak width and the coexistence of both orientations. The inset of Figure 1, lower panel shows the (100) and the ($\underline{1}$10) orientations of the orthorhombic unit cell. In this orientation, the polymer chain axes along the orthorhombic *c*- or (001) axis lie in the film plane. The electric polarization vector is parallel to the orthorhombic *b* or (010) axis. The hexagon in the figure indicates the six allowed polarization orientations, meaning the orthorhombic unit cell reorients together with the polarization vector.

According to the PFM measurements reported below, the polarization in our poled films is always along one of the four directions forming an angle of 30° with the film normal that are characterized by a large vertical PFM response. In other words, only the orthorhombic ($\underline{1}$10) orientation has been observed. The measured shift of the ($\underline{1}$10) peak hints at a possible reason for this. Assuming a stoichiometric film, the shift reveals an elastic film strain with vertical compression and in-plane expansion. Since the lattice of PVDF-TrFE shortens along the polarization direction at the paraelectric-to-ferroelectric transition (see Section 2.4), the canted vertical polarization orientation is the more favorable one.

The crystalline in-plane orientation of the film is crucial for the measurable piezoresponse that is weak along the polymer chain axis (*c*-axis) and largest along the polarization axis (*b*-axis).[30] In our films with thicknesses between 50 and 150 nm, the crystalline lamellae with an average width between 25 and 30 nm show randomly distributed in-plane orientations (for AFM and SEM images, see ref. [29] and Figures S1, S4, and S8 (Supporting Information)). The random in-plane orientation is consistent with the fact that no in-plane anisotropy in the domain writing experiments could be detected. The polymer chain axis, i.e., the (001) direction, is roughly perpendicular to the crystalline lamellae that stand "on-edge" (Figure 1a, inset). It is useful noting that ultrathin PVDF-TrFE films can grow fully oriented (i.e., epitaxially) on graphite,[16] defining three in-plane orientations for crystalline lamellae. In our films, local patches still revealing the preferred in-plane orientations of lamellae have been occasionally detected using atomic force microscopy.

2.2. Deterministic Writing of Four Polarization Directions

We show here that the four polarization directions indicated in Figure 2d can be deterministically set within defined areas using piezoresponse force microscopy (vertical PFM (VPFM) and lateral PFM (LPFM)). The pristine films are found to be in a multidomain state without detectable self-poling. This can be seen in the surrounding areas of written domains in **Figures 2–5**, where no well-defined VPFM and LPFM phases and low PFM amplitudes are present. First, the vertical polarization component is defined by scanning the force microscopy tip with an applied electric voltage. Here, positive and negative electrical poling with ± 10 V is applied in neighboring rectangular areas; the phase image of the vertical piezoresponse (Z_{ph}) is shown in Figure 2a. The uniform phase contrast (and the large PFM amplitude, Figure S9, Supporting Information) indicate efficient vertical poling which excludes a horizontal polarization direction in the pseudohexagonal lattice (Figure 2d). Any artificial enhancement of the VPFM signal caused by injected charge from the tip to the sample surface can be excluded (Figure S6, Supporting Information and discussion in ref. [29]). Subsequently, the electrically grounded tip is used to scan smaller quadratic areas with an enlarged tip force of 200 nN as indicated in Figure 2b. The open white arrows mark the slow-scan direction of the tip that scans in back-and-forth mode.[29] With this "mechanical poling" step, the in-plane polarization component is efficiently oriented as visible in the LPFM phase image, Figure 2c. It is set parallel (antiparallel) to the slow-scan

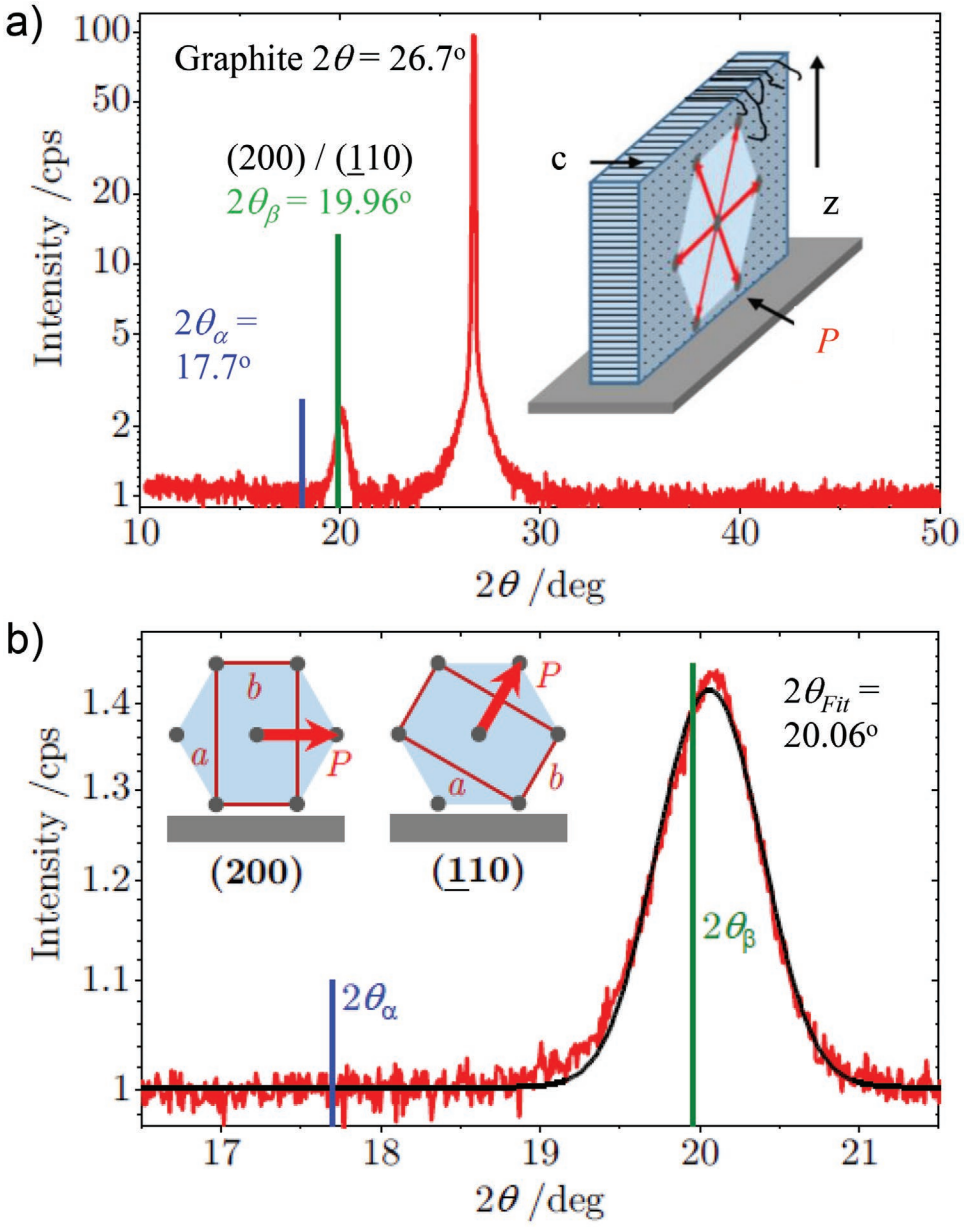

Figure 1. X-ray diffraction θ–2θ scan of a representative PVDF-TrFE film after subtracting the substrate background signal. Peak positions of unstrained α– and β-phases are marked. a) Wide-angle scan for checking phase purity. The inset shows a scheme of a crystalline lamella with the crystallographic c-axis parallel to the substrate plane and the short lamella direction. b) Expanded view around the first-order (200)/(1̄10) peak. The inset illustrates the two crystalline orientations of the β-phase and the related polarization orientations.

direction for the electrically positively (negatively) poled rectangle (Figure 2c,d). Hence, the vertical poling defines the sign of the achieved in-plane polarization component. We note that all panels of Figure 2 have been recorded after the mechanical treatment. The four polarization orientations sketched in Figure 2d have been set in the quadratic domains of about $2 \times 2\ \mu m^2$ size (Figure 2c).

The phase images like Figure 2c indicate the dominating in-plane polarization orientation averaged over an area under the tip and the depth of the film. For film thicknesses investigated here (50–150 nm), the electric field penetrates the entire film with same order of magnitude; hence, the PFM signals originate from the entire depth of the film. The completeness of the in-plane poling cannot be evaluated from phase images alone. For this purpose, the magnitude of the in-plane (LPFM) amplitude can be used to evaluate the degree of dipole order. In Figures S5 and S9 (Supporting Information), off-resonant measurements of LPFM and VPFM signals are shown including amplitudes. The VPFM amplitude is ≈22 pm V^{-1}, the LPFM amplitude ≈75 pm V^{-1}. The LPFM signal contains contributions from piezoelectric coefficients d_{33}, d_{31}, and d_{15}, which are all of similar high magnitude (30–34 pm V^{-1}) in the used PVDF-TrFE.[31] Therefore, one can do a simple estimation based on the tilt angle of the polarization. The tilt

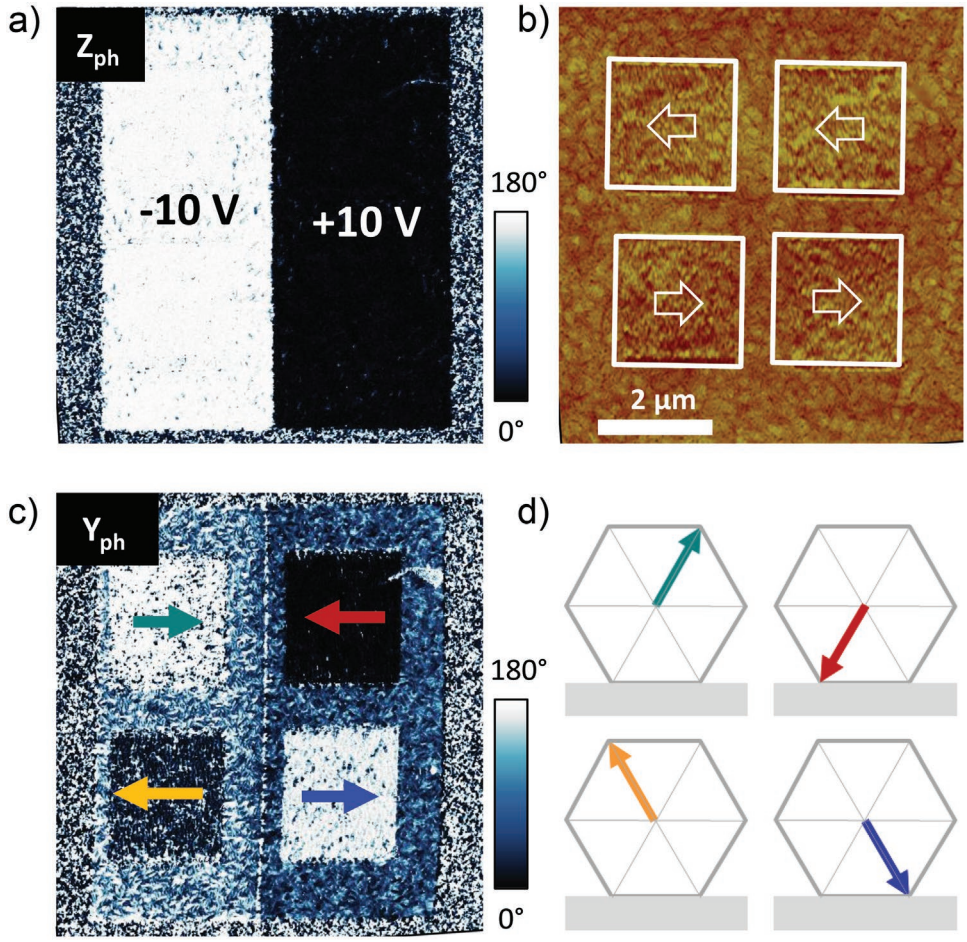

Figure 2. Defining four polarization orientations. a) Two rectangular areas were electrically poled with a tip voltage of ±10 V (phase contrast of the vertical piezoresponse). b) Topographic AFM image after the mechanical treatment. Four quadratic areas have been scanned with a tip force of 200 nN and an electrically grounded tip. White arrows indicate the slow-scan direction along the in-plane *y*-axis. c) Phase contrast of the lateral piezoresponse along the in-plane *y*-axis (Y_{ph}). Colored arrows indicate the polarization orientation which is schematically shown in (d).

angle of the polarization vector with the measured direction reduces the expected PFM amplitude by cos(30°) = 0.866 and cos(60°) = 0.5 for VPFM and LPFM amplitudes, respectively. Additional reduction for the LPFM signal results from random in-plane orientation of lamellae which accounts for a reduction factor of ≈0.7. Considering these reductions from polarization tilts, the expected ratio of LPFM and VPFM amplitudes is ≈0.4, while the measured ratio is 0.34. This indicates that the lateral poling has been nearly as efficient as the vertical poling and is not a surface phenomenon.

There is no significant surface roughening or disturbance of the vertical poling if the tip force has been chosen appropriately. The rms roughness typically increases by 1–2 nm. The applied vertical force leads to a shear stress estimated as the product of the normal stress and the friction coefficient[22,32]; this gives a shear stress of ≤15 MPa for the mechanical poling experiments reported here. We note that the friction force of the tip appears to be independent of the tip velocity, since the magnitudes of both, the fast-scan-velocity and the slow-scan-velocity have shown negligible impact on the poling efficiency in their readily accessible range (Figures S13 and S14, Supplementary Information).

2.3. Writing Complex Nanoscale Domain Patterns

The mechanical poling can be applied to define more complex nanoscale domain patterns. Three examples in Figures 3–5 illustrate the versatility of the approach. An image consisting of black and white "bits" can be defined in the vertical polarization using a biased tip and copied to the in-plane polarization by a subsequent mechanical scan with constant force (Figure 3). Figure 4 demonstrates an alternative approach of direct mechanical writing of a pattern into a uniformly poled area. Figure 5 shows the option of defining in-plane polarizations at deliberate angles.

In more detail, the domain pattern in Figure 3 is achieved by electric writing using the scanning tip with controlled electric voltage of +10 or −10 V, respectively. This sets the out-of-plane polarization component according to the desired image. In a subsequent scan with grounded tip and constant mechanical force of 200 nN, the pattern is transferred into the in-plane polarization as sketched in Figure 3a. The resulting domain walls are 180° walls, since opposite vertical polarization leads to opposite lateral polarization in a uniform mechanical scan.

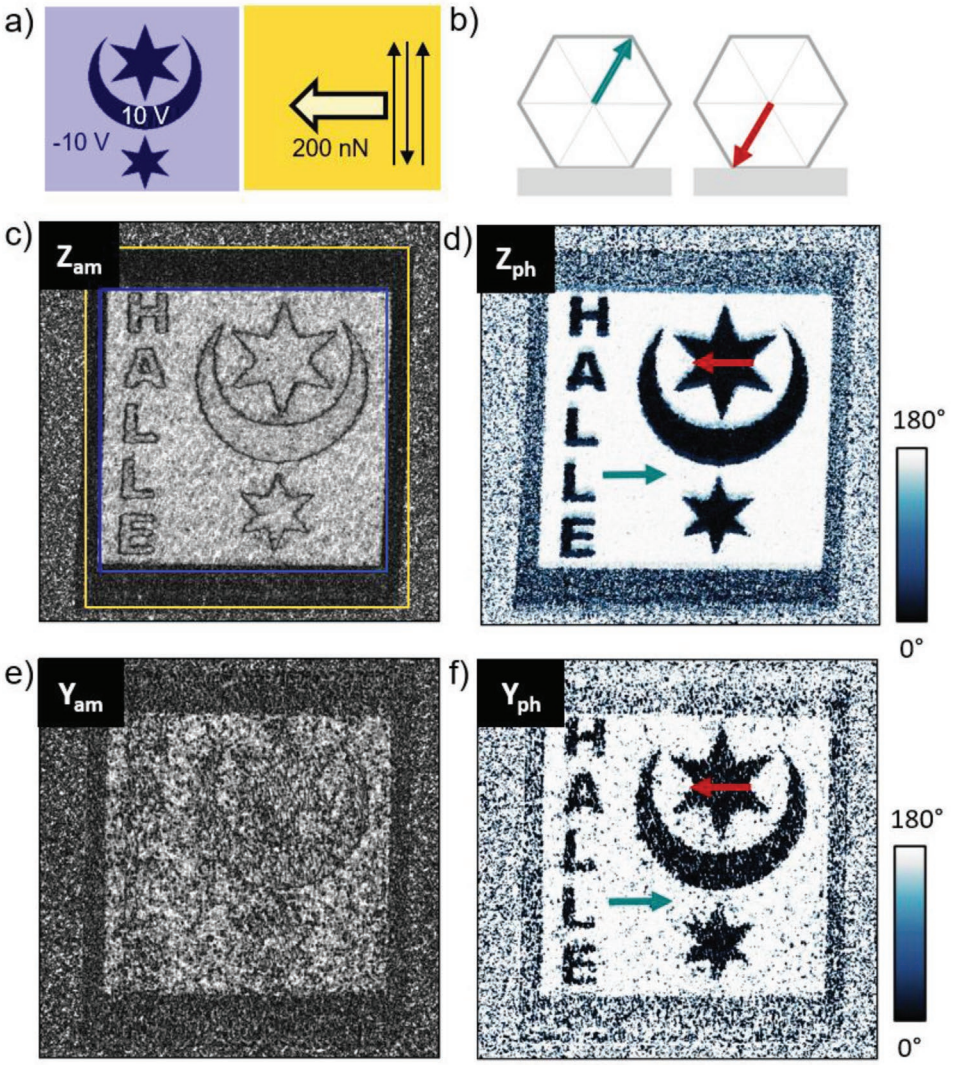

Figure 3. Ferroelectric domain pattern written with electric tip voltage and subsequent mechanical transfer into the in-plane polarization. a) Schematics of the writing process. Electric poling as indicated in the blue frame is followed by a uniform mechanical scan (yellow frame) with unbiased tip and 200 nN tip force. b) Scheme of polarization orientations. c) Vertical piezoresponse amplitude and d) associated phase. e) Lateral (along *y*-direction) piezoresponse amplitude and f) associated phase. Polarization orientations in (d,f) marked by colored arrows. PFM measurement in on-resonance mode. The resulting domain walls are of 180° type.

In Figure 4, a uniformly poled area (obtained like those in Figure 2) is used to mechanically write the pattern with a tip force of 200 nN that is switched on and off according to the pattern during scanning. Thus, the pattern is defined purely mechanically. There is some resemblance to writing with a pencil. In contrast to Figure 3, the resulting domain walls are 60° walls here, because the vertical polarization component remains unchanged. The slightly lower in-plane PFM amplitude (Y_{am}) in some parts of the pattern (Figure 4e) reveals where the mechanical reversal of the in-plane polarization was not fully complete. The choice of the appropriate force is vital: too low force will fail to switch the polarization, while too large force tends to damage the film (as has happened at the right edge of the large poled area in Figure 4).

In Figure 5, a Landau domain pattern has been written with four different in-plane polarization directions. In analogy to the electrical poling of a polycrystalline medium, any in-plane direction can be chosen for poling, under the condition that grains are small enough and randomly oriented. The vertical polarization component points downward in Figure 5, which is the more stable vertical polarization orientation. The phase images (Figure 5e,g) show a white and a dark triangle where polarization is parallel to the measured in-plane direction. In these areas, a strong amplitude enhancement is observed (Figure 5d,f). The phase in the triangles with the polarization perpendicular to the measured direction appears inhomogeneous and the amplitude in these areas is low, leading to the ill-defined phase. The images in Figures 5d,f with identical amplitude scaling indicate similar piezoresponse enhancements after mechanical poling for the two orthogonal in-plane directions, confirming the absence of in-plane anisotropy (Section 2.1). We note that it is possible to define any angle between in-plane polarizations of two adjacent domains.

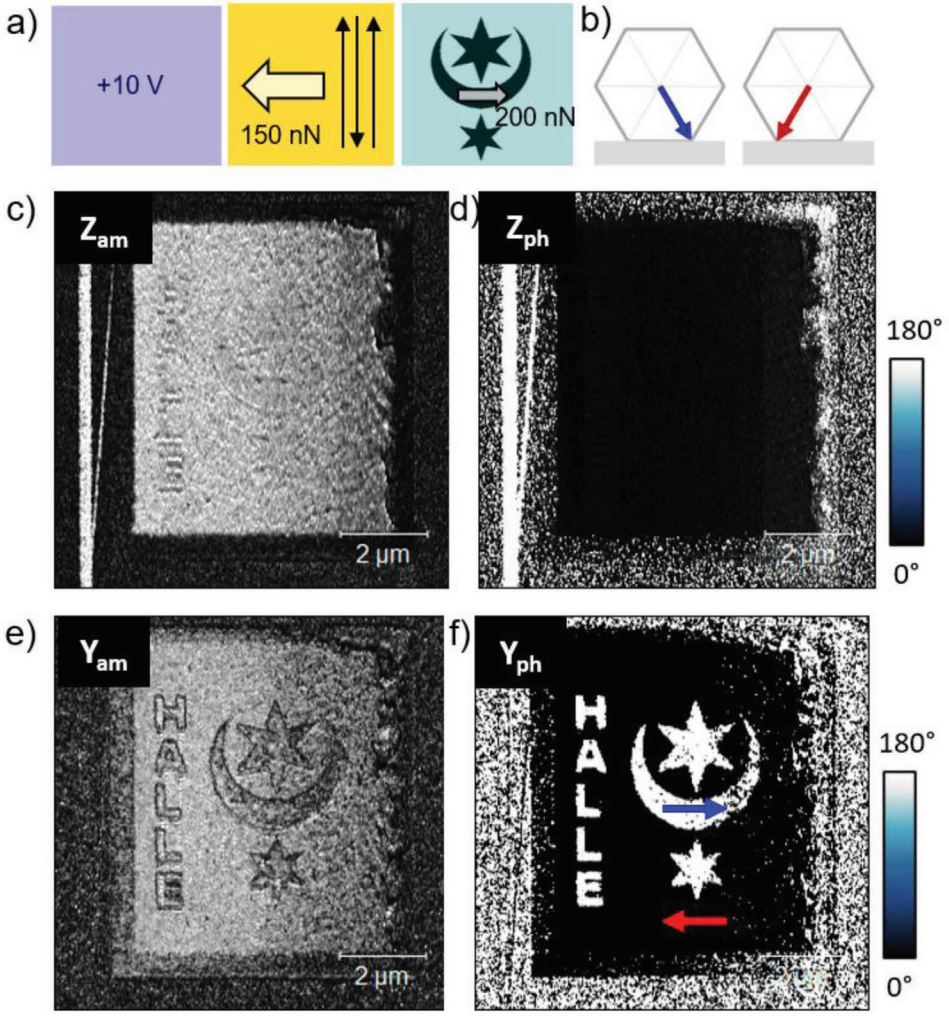

Figure 4. Ferroelectric domain pattern written mechanically after uniform electric poling. a) Schematics of the writing process. Electric poling (blue frame) followed by a uniform mechanical scan (yellow frame) followed by mechanical pattern writing (achieved by controlling the tip force). b) Scheme of polarization orientations. c) Vertical piezoresponse amplitude and d) associated phase. e) Lateral (along *y*-direction) piezoresponse amplitude and f) associated phase. Polarization orientations in (f) marked by colored arrows. PFM measurement in on-resonance mode. The resulting domain walls are of 60° type. The right edge of the written area shows damage resulting from the mechanical scan.

The written domain patterns show feature sizes down to ≈60 nm that is about the tip diameter. Thus, the resolution limit of the mechanically written domains results from the tip size. On the other hand, the width of crystalline lamellae is important. This can be expected, because the polarization can align only along six fixed directions inside a given lamella. The systematic impacts of tip size and lamellar microstructure yet need to be explored. A distinct advantage of mechanical domain writing over electrical domain writing is the avoidance of electrical stray fields. The latter prevent the writing of such small domains with defined in-plane polarization in PVDF-TrFE using the tip-trailing field, because required electric fields and, thus, stray fields, are too large.

2.4. Mechanical Switching Mechanism

Here, we attempt to elucidate the physical mechanism of the mechanical switching. In previous work it was shown that no structural reconstruction/crystalline reorientation like the one introduced in ref. [22] takes place for the medium tip forces applied here, apart from a very thin surface layer.[29] Further potential mechanisms are the ferroelastic effect and the flexoelectric effect,[33] since the tip force causes mechanical strains and strain gradients in the polymer film. Flexoelectricity can be ruled out as the driving force, since the vertical polarization orientation determines the sign of the mechanically defined in-plane polarization component (Figure 2). Mechanical strain gradients and the resulting proportional electric field caused by flexoelectricity are independent of a previously defined polarization orientation.

The coupling of strain and polarization is possible through a ferroelastic effect. Reports on ferroelastic phenomena of PVDF-based polymers are yet very scarce.[34,35] If the lattice is elongated/shortened along the polarization direction, straining a ferroelectric crystal can reorient the polarization. For example, the polarization is parallel to the long *c*-axis in tetragonal

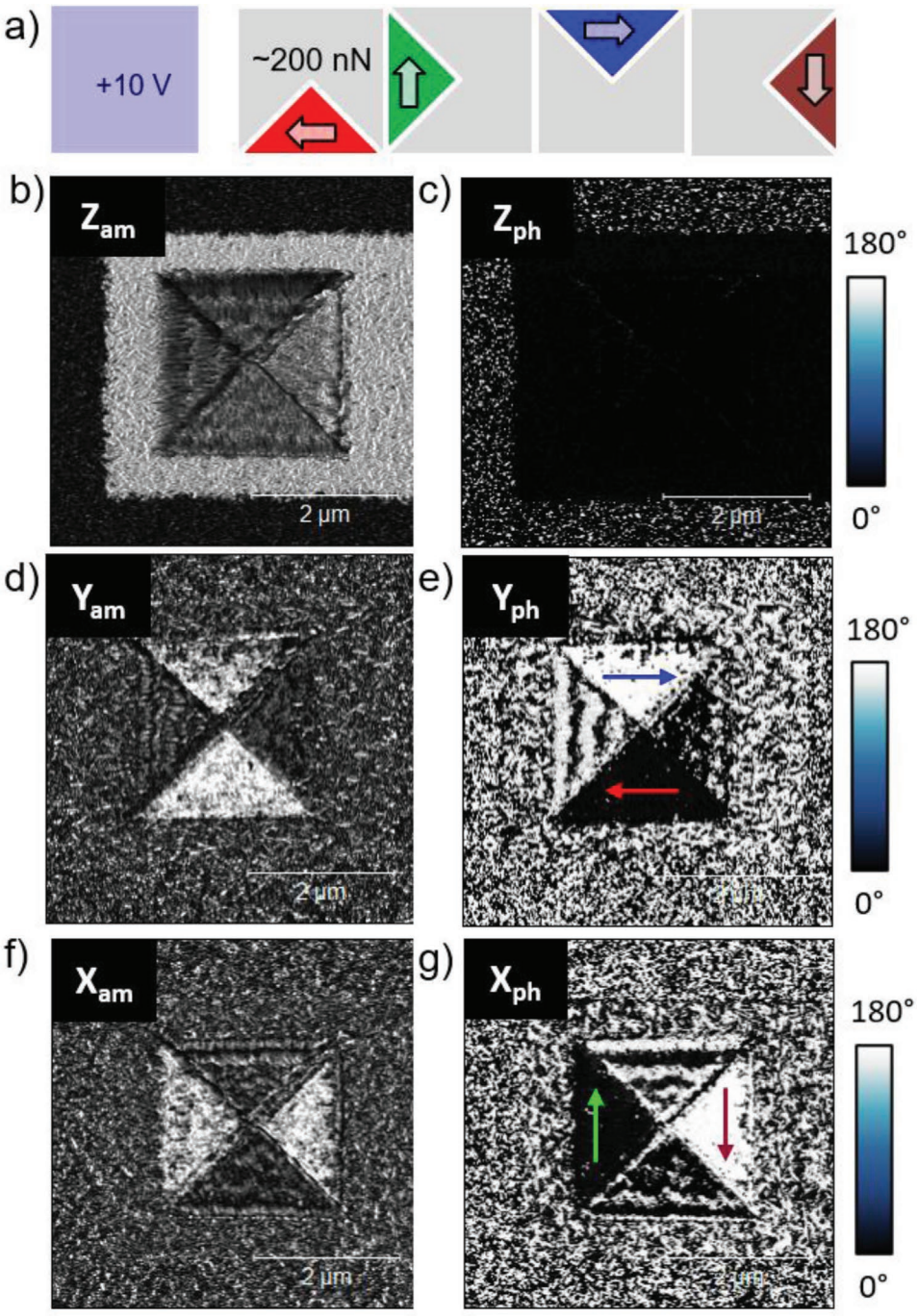

Figure 5. Ferroelectric Landau domain pattern with four in-plane polarization directions. a) Schematics of the writing process. Electric poling (blue frame) is followed by four mechanical scans in triangular areas as indicated. The open arrow marks the slow-scan direction. b) Vertical piezoresponse amplitude and c) associated phase. Lateral (along *y*-direction) d) piezoresponse amplitude and e) associated phase. Lateral (along *x*-direction) f) piezoresponse amplitude and g) associated phase. Polarization orientations in (e, g) marked by colored arrows. PFM measurement in on-resonance mode. Note the larger piezoresponse (bright contrast) in the triangular areas where the average polarization is aligned along the measuring direction.

ferroelectrics like $PbZr_{0.2}Ti_{0.8}O_3$. Reorientation of the *c*-axis by mechanical force is associated with polarization reorientation. For mechanically flexible polymers, the situation is favorable for the observation of mechanically induced switching due to their softness. Importantly, this strain-driven polarization switching that we will refer to as "ferroelastic" subsequently cannot determine the sign of the polarization. This agrees with our experimental result, where the electrically set vertical polarization component defines the direction of the mechanically induced in-plane polarization component (Figure 2).

The hexagonal paraelectric phase transforms to the orthorhombic phase with the polarization oriented along the orthorhombic *b*-axis (Figure 1, inset) at the Curie temperature ($T_C \approx 125$ °C). A neutron diffraction study of the crystallographic structure evolution with TrFE contents of 0–40% conducted by Bellet-Amalric[36] reveals a systematic increase in the orthorhombic distortion $H = a/(\sqrt{3}b) - 1$ with the TrFE content. They find H = 1.7% at 20% TrFE and H = 2% at 30% TrFE, while H = 0 in the hexagonal phase. This indicates a shortening of the *b*-axis along the electric polarization of ≈1.7% in our samples with 22% TrFE. Interestingly, also the piezoelectric coefficient along the polarization direction (d_{33}) is negative,[30,37] revealing a lattice shortening in an electric field parallel to the polarization. This is in contrast to most oxide ferroelectrics (like the above mentioned $PbZr_{0.2}Ti_{0.8}O_3$) that elongate along the polarization direction and also show $d_{33} > 0$.

Before addressing the switching mechanism on the basis of stress/strain in the crystalline phase, the role of the amorphous phase should not be ignored. Recent work demonstrated a substantial contribution of the amorphous phase to the measured total piezoelectric effect.[37,38] Katsouras et al. found electromechanical coupling of crystalline and amorphous phases resulting in an additive contribution to the piezoelectric coefficient d_{33}.[37] The amorphous phase in the present work amounts to ≈40% of the film volume.[29] Therefore, we expect the amorphous phase to be essential for the quantitative mechanical reaction of the polymer film in the reported mechanical domain writing/poling experiments. Nevertheless, we believe the physical mechanism can be qualitatively captured by considering the effect of stress/strain in the crystalline phase. The amorphous phase is much softer as seen, for example, in a logarithmic elasticity modulus image Figure S1d (Supporting Information).

Figure 6 summarizes the suggested ferroelastic switching mechanism. Electrical downward poling of the polarization is applied prior to the mechanical scan, resulting in two possible P orientations with opposite in-plane component (Figure 6a). In Figure 6b, the back-and-forth scan is visualized as a top view. (Note that the component of the fast-scan-velocity (v_f) that is parallel to the lamellae has no poling effect. This is addressed below (**Figure 7**b). According to our experiments, the in-plane polarization orients along the slow-scan direction (Figure 6b). The line distance has been varied between 8 and 63 nm; most efficient mechanical poling was observed with a line distance slightly smaller or similar to the tip radius (i.e., for 15 and 31 nm, Figure S12, Supporting Information). The fast-scan velocity was varied between 0.75 and 37 µm s^{-1} without systematic influence on the poling result (Figure S14, Supporting Information). The slow-scan velocity (v_s) had no impact on the poling quality, too, between 10 and 75 nm s^{-1} (Figure S13, Supporting Information). The qualitative strain distribution in a homogeneous medium is illustrated as a top view (Figure 6c) and a cross section view (Figure 6d). We use the homogeneous medium as first approximation, aiming at a qualitative understanding. The moving tip that is approximated as a sphere induces a pressure ($\sigma > 0$) in front of it and, due to adhesion of the polymer at the tip, a pull or negative pressure behind it (Figure 6c). The negative pressure is directed roughly toward the center of the tip. The consequence is an elongation in this direction. The elongated direction is less favorable for the polarization which is, thus, reoriented in the other available direction which is pointing toward the scan track (Figure 6d). Figure 6e illustrates the effect of the slow-scan velocity that is

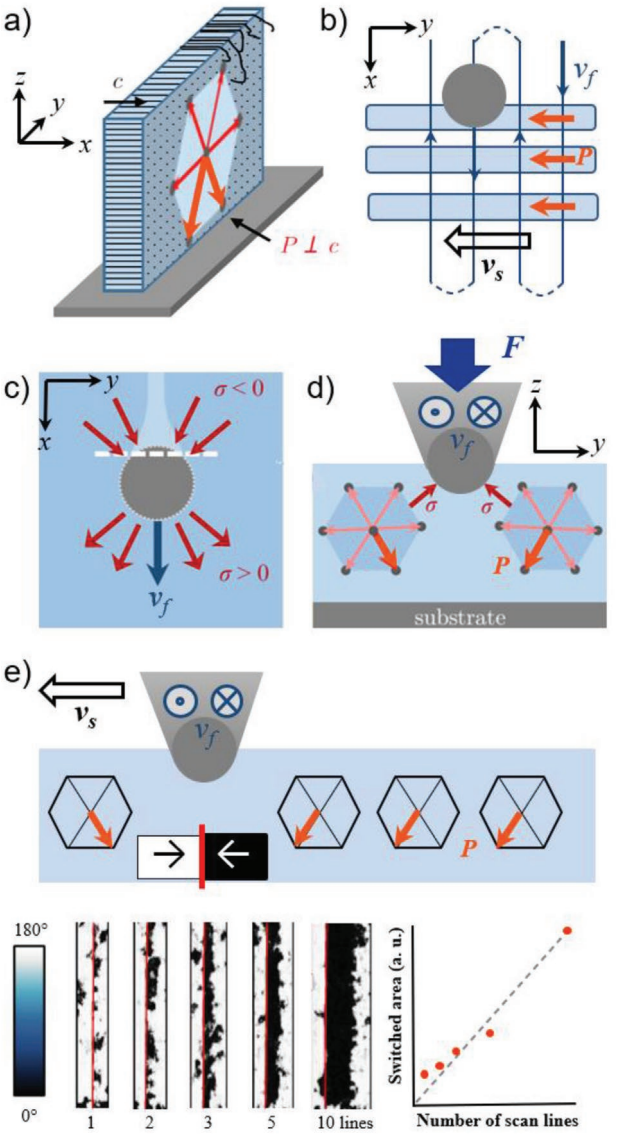

Figure 6. Mechanical switching by moving force microscopy tip. a) Scheme of a crystalline lamella. After positive electric poling, the two polarization orientations looking downward (fat bright-red arrows) are present. b) Top view of three lamellae with indicated tip (grey sphere) motion. The fast-scan velocity (v_f) is perpendicular to the lamellae. The v_f component along the lamellae can be neglected (see the text). The slow-scan velocity (v_s) sets the polarization parallel to it in the same direction. c) Top view in a continuum model. The moving tip causes positive stress ($\sigma > 0$) in front of it. Due to the adhesion of the polymer to the tip, the stress behind the tip is negative. d) Cross-section view of the tensile stresses behind the moving tip. The polarization reorients toward the track in order to avoid the elongated lattice direction. e) Scheme of the overwriting along the slow-scan direction (top panel) and experimental images with increasing number of fast-scan lines with a tip force of 150 nN (bottom panel). The red line marks the last tip track. The line distance in 20 nm. The bottom right panel shows the switched (black) area per number of scan lines. The grey line sketches a proportional relation expected for large line numbers.

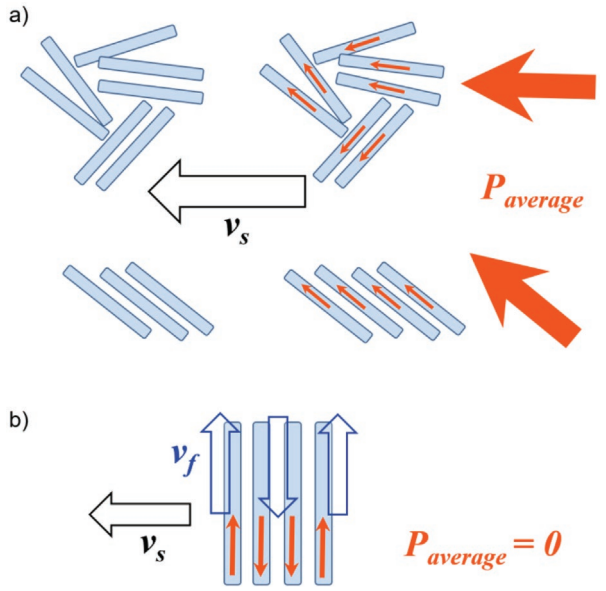

Figure 7. Influence of an in-plane texture. a) Random and fully aligned in-plane orientation of lamellae sketched in top and bottom parts, respectively. The indicated slow-scan direction (after positive electric poling) results in the marked polarization directions in the individual lamellae. The averaged polarization ($P_{average}$) is oriented as shown on the right side. Hence, an in-plane texture causes a deviation between the directions of the slow scan (v_s) and the averaged in-plane polarization ($P_{average}$). b) Cancellation of mechanical poling effect for back-and-forth scans of the fast-scan velocity (v_f) parallel to the crystalline lamellae.

simply an overwriting effect. This is in resemblance to the electric tip-trailing effect.

Experimentally, we explored the accumulating effect of scanning single lines with the tip (Figure 6e, bottom). The lines were scanned with a tip force of 150 nN and a line distance of 20 nm in a nearly uniformly poled area (white, polarization points right). A few domains with polarization "left"—black phase contrast—were present before the scan. Red lines mark the center of the tip tracks. The in-plane polarization reorients toward the track in some places after the first line scan (black patches on the right side of the red line). The orientation on the left side of the red line remains unchanged (white). For a single line, the poling is only partial, but it becomes clearer with repeated line scans. Repeated parallel line scans enlarge the black area and result in uniform black contrast eventually (Figure 6e, bottom). The "obstacles" caused by the inhomogeneous microstructure are thus overcome by the repeated scans. The in-plane polarization is gradually aligned and points in the slow-scan direction. In other words, the slow-scan direction leads to overwriting of one of the in-plane P orientations created by single line scans (Figure 6e). We note that the reversal of the fast scan direction has no influence; scans have been performed both in back-and-forth mode and in forward-only mode. After negative electric poling, the in-plane polarization reverses, i.e., it points away from the scan line always.

This proposed ferroelastic switching mechanism (Figure 6) is consistent with all of our experiments. We note that the poling mechanism suggested here is independent of the presence of an in-plane texture in the polymer film. However, the true orientation of the in-plane polarization must depend on the crystallographic texture, since P is parallel to the long lamella extension (i.e., perpendicular to the *c*-axis) and the slow-scan direction just selects one of the two possible P orientations inside each lamella. Hence, the in-plane texture governs the distribution of local polarization and the averaged in-plane polarization $P_{average}$ (Figure 7a). In our experiments, the in-plane direction orthogonal to v_s most often showed a negligible piezoresponse, indicating that the averaged polarization component in that direction was very small as a consequence of disordered lamellar in-plane orientations. This is in contrast to expectations for an epitaxial film with aligned lamellae as sketched in the lower part of Figure 7a, where both in-plane polarization components would be ordered, since they are not independent. Finally, Figure 7b visualizes the reason why the fast-scan-velocity component parallel to the lamellae has no aligning effect on the averaged polarization. The back-and-forth motion of the tip results in alternating polarization directions that cancel out. An open question remains if unidirectional line scans parallel to lamellae (only the forward motion of the tip done under mechanical load) could achieve a mechanical poling effect.

The ferroelastic effect of PVDF (with copolymers) is yet very little investigated. It is highly desirable to develop a more quantitative model of the observed mechanical switching phenomenon. Toward this goal, the anisotropic properties of crystalline lamellae, their (in-plane) texture and the amorphous phase between lamellae need to be included in order to address the mechanical behavior of the polymer films. An easier scenario may arise for bulk effects when the mechanical stress is constant in regions containing a large number of lamellae such that effective mechanical properties can be used for the polymer.

2.5. Thin-Film Device Functionalities

Finally, we suggest options how the aligned in-plane polarization component in PVDF-TrFE films might be utilized for device functionalities. The long-term stability of domains written in the PVDF-TrFE films is extremely good, we find that domains can keep their detailed nanoscale features for at least 4 years (Figure S10, Supporting Information). The samples have been stored in a dehydrated atmosphere at ambient temperature. The large ferroelectric-to-paraelectric Curie temperature of 125 °C, the stability of the β phase for the used PVDF-TrFE copolymer composition and the absence of itinerant ions like oxygen in oxide ferroelectrics might account for the observed domain stability that is not well understood at present. We note that there are other reports of excellent long-term stability of the piezo- and pyroelectric responses.[39,40] Robust polarization stability has recently been reported also for films grown on monolayer graphene oxide.[15]

This long-term stability is beneficial for using domains in memory applications. The deterministic setting of four polarization directions demonstrated here provides a foundation for a four-state-memory. An example showing the storage of two independent images in the same place is given in the Figure S15 (Supporting Information). Two-state memory

applications of PVDF-TrFE films exploiting the vertical polarization component have been investigated for some time.[9–12] As an example of a resistive-switching memory device, electric switching of the in-plane polarization component in PVDF-TrFE was recently demonstrated in planar ferroelectric tunnel junctions.[41] The switching polarization charge can be as high as ± 11 μC cm^{-2} if textured films with horizontal polarization could be used; for random lamellae orientation, this value is reduced to about ± 4 μC cm^{-2}.[37]

Another essential aspect is the energy consumption for mechanical polarization switching. For our samples, an electric poling step was required before setting the in-plane polarization component with mechanical force. This process requires more energy than electric switching alone, namely the electric energy for vertical poling and the mechanical energy for lateral poling. It would be much more favorable with self-poled PVDF-TrFE films that may permit to eliminate the electrical poling step and make the energy consumption of mechanical switching competitive to electrical switching.

Exploiting the direct piezoelectric effect, PVDF-TrFE is used as the active component in thin-film pressure sensors as well as in energy-harvesting devices. There, the polymer layer is sandwiched between electrode layers for the vertical measurement of the pressure-induced piezoelectric voltage. An aligned in-plane polarization component additionally results in an in-plane piezoelectric voltage in response to a pressure acting perpendicular to the film surface. (For a disordered in-plane polarization, the in-plane piezoelectric voltage is suppressed by cancellation of local voltage responses.) Thus, the ordered in-plane polarization enables building pressure sensors with two top electrodes on a polymer film/membrane instead of using electrode/polymer/electrode sandwich structures. Further, it may be favorable for certain applications that top electrodes can be repositioned on demand. Actuators based on the inverse piezoelectric effect (i.e., elastic strain driven by an applied voltage) may also benefit from a top-electrodes configuration.

Moreover, inhomogeneous pressure distributions could be detectable. Local strains in a PVDF-TrFE film transfer into local electrical fields through the piezoelectric effect. The field distribution could be imaged, for example, optically through the Kerr effect (the light polarization rotation of linearly polarized light). In a PVDF-TrFE membrane with uniform polarization poling, the strain distribution could be probed and imaged using a light interference approach.

As a final suggestion, a domain pattern written into a PVDF-TrFE film may be used to create an electrical potential distribution upon application of uniform pressure perpendicular to the film plane. The electrical potential distribution can be "reprogrammed" by mechanical domain writing. There is no consumption of electrical energy to keep up the electrical potential distribution, in contrast to an electrical circuit producing the same potential distribution.

The options for up- or down-scaling of the mechanical poling approach are yet hard to evaluate. For a smaller domain size, a smaller force microscopy tip must be employed and the lamellar microstructure will be essential. Very small, thin, and densely packed lamellae with random in-plane orientation are required to allow for writing even smaller domains (<50 nm) with deliberate in-plane polarization orientation. For up-scaling, we roughly estimate the applied tip pressure as 5×10^7 Pa or 500 bar, assuming a tip radius of 35 nm and a force of 200 nN resting on the area of a circle with the tip radius. This indicates that an existing domain pattern in PVDF-TrFE is stable against common mechanical handling. By sufficiently large pressure of the order of 500 bar, the polarization axis could be set along the pressure axis. Controlling the sign of the polarization, however, cannot be achieved with a ferroelastic effect. It needs either an additional electrical field (like in this work) or an electrically self-poled film. Further, the pressure estimation is not capturing the complete mechanical effect of a moving tip that stretches the material behind the tip due to adhesive forces between polymer and tip. Polarization switching by the pressure of an unmoving tip has been tested, too, and works with about the same tip force (Figure S11, Supporting Information).

3. Conclusions

Thin films of (110)-oriented PVDF-TrFE (22 mol-% TrFE) with thicknesses of 50–150 nm have been prepared on graphite. They consist of ferroelectric β-phase in densely packed crystalline lamellae of <30 nm width that have no detected in-plane texture. After the film has been electrically poled perpendicular to the film plane, a moderate mechanical force exerted by a moving force microscopy tip has been used to align the in-plane polarization component in the film along a deliberately chosen direction. In analogy to the electric poling of a polycrystalline material, this previously unknown effect could be called "mechanical poling." Complex domain patterns with well-defined domain features down to 50 nm have been written in films of up to ≈150 nm thickness. The surface roughness typically remains below rms ≈3 nm after a mechanical scan. The domain patterns have been found to be stable for several years. We discussed a ferroelastic origin for the mechanical polarization switching that is based on the lattice shortening along the polarization direction (the orthorhombic *b*-axis). Finally, we proposed ways to exploit mechanically defined polarization patterns in thin film devices.

4. Experimental Section

Thin films were prepared by spin coating a 2 wt.% solution of PVDF-TrFE granules (Piezotech, measured composition of 22 mol-% TrFE) in 2-Butanone on highly ordered pyrolytic graphite (HOPG) glued on silicon substrates. The spin-coated film was subsequently annealed at 180 °C, slightly above the melting temperature, for 30 min in vacuum (10^{-3} mbar) and quenched on a large metal plate to room temperature. Phase transition temperatures for this composition had been reported in ref. [18]. The investigated film thicknesses ranged from 50 to 150 nm and might locally vary in a given film by up to 20%. Local film thickness was measured in a force microscope using a topographic scan after removing the film with the tip (creating a substrate-deep hole). X-ray diffraction measurements were taken in a Bruker Discover D8 diffractometer using Cu Kα_1 radiation.

Atomic force microscopy (AFM) and piezoresponse force microscopy (PFM) were carried out using both, a MFP-3D (Asylum Research) and a NTEGRA Aura (NT-MDT) microscope. For mechanical writing, a vertical force in the range of 100–300 nN was applied with a Pt/Ir-coated AFM-tip (HQ:CSC17-Pt, MikroMasch, tip radius ≈35 nm, force

constant ≈0.2 N m $^{-1}$) to the polymer film in contact mode. The same tip was used for electric poling. If not stated otherwise, mechanical scanning was performed with scan line distances of ≈20 nm with the slow scan direction parallel to the cantilever orientation, pulling the cantilever "backwards," and scanning speed of ≈2.5 µm s^{-1}. The force was adjusted using the cantilever deflection signal multiplied by the inverse optical lever sensitivity and the cantilever spring constant. (The lever sensitivity was obtained by measuring force distance curves. The spring constant was determined by measuring the thermal noise of the cantilever at resonance frequency and calculating the spring constant using the equipartition theorem of a simple harmonic oscillator.) All PFM images were taken with tip force below 40 nN in resonant (DART) or off-resonant modes as indicated for the respective measurements. For imaging both in-plane directions, samples could be rotated by 90°.

Supporting Information

Supporting Information is available from the Wiley Online Library or from the author.

Acknowledgements

The authors thank T. Thurn-Albrecht, G. Catalan, M. Ghidini, and N. Mathur for inspiring and clarifying discussions. Samples were prepared in collaboration with T. Thurn-Albrecht. This work had been funded by Deutsche Forschungsgemeinschaft within the Collaborative Research Centers CRC 762 Functionality of oxide interfaces (A8) and TRR 102 Polymers under multiple constraints (B3).

Open access funding enabled and organized by Projekt DEAL.

Conflict of Interest

The authors declare no conflict of interest.

Author Contributions

R.R. and K.D. conceived the idea of this work. M.M.K. prepared the samples. A.D.R. and M.M.K. performed the X-ray measurements. R.R. performed all force microscopy work. R.R. and K.D. analyzed the data, derived the results, and wrote the manuscript with assistance of all authors.

Data Availability Statement

The data that support the findings of this study are available from the corresponding author upon reasonable request.

Keywords

domains, ferroelectric, ferroelastic, force microscopy polymer, PVDF, strain

Received: December 31, 2021
Revised: March 3, 2022
Published online: April 20, 2022

[1] S. Azimi, A. Golabchi, A. Nekookar, S. Rabbani, M. H. Amiri, K. Asadi, M. M. Abolhasani, *Nano Energy* **2021**, *83*, 105781.
[2] R. A. Surmenev, R. V. Chernozem, I. O. Pariy, M. A. Surmeneva, *Nano Energy* **2021**, *79*, 105442.
[3] K. Lu, W. Huang, J. Guo, T. Gong, X. Wei, B.-W. Lu, S.-Y. Liu, B. Yu, *Nanoscale Res. Lett.* **2018**, *13*, 83.
[4] U. Yaqoob, A. S. M. I Uddin, G.-S. Chung, *Appl. Surf. Sci.* **2017**, *405*, 420.
[5] F. R. Fan, W. Tang, Z. L. Wang, *Adv. Mater.* **2016**, *28*, 4283.
[6] V. Bhavanasi, V. Kumar, K. Parida, J. Wang, P. S. Lee, *ACS Appl. Mater. Interf.* **2015**, *8*, 521.
[7] J. Liu, Q. Zhao, Y. Dong, X. Sun, Z. Hu, H. Dong, W. Hu, S. Yan, *ACS Appl. Mater. Int.* **2020**, *12*, 29818.
[8] K. L. Kim, M. Koo, C. Park, *Nanoscale* **2020**, *12*, 5293.
[9] Y. Chen, X. Chen, H. Lu, L. Zhang, Y. Yang, Q.-D. Shen, *Polymer* **2018**, *143*, 281.
[10] X. Chen, X. Tang, X.-Z. Chen, Y.-L. Chen, X. Guo, H.-X. Ge, Q.-D. Shen, *Appl. Phys. Lett.* **2015**, *106*, 042903.
[11] S. J. Kang, I. Bae, Y. J. Shin, Y. J. Park, J. Huh, S.-M. Park, H.-C. Kim, C. Park, *Nano Lett.* **2011**, *11*, 138.
[12] Z. Hu, M. Tian, B. Nysten, A. M. Jonas, *Nat. Mater.* **2009**, *8*, 62.
[13] G. Strobl, *The Physics of Polymers*, 2nd ed., Springer, Berlin, Germany, **2007**.
[14] C. Zhao, Y. Hong, X. Chu, Y. Dong, Z. Hu, X. Sun, S. Yan, *Materials Today Energy* **2021**, *20*, 100678.
[15] P. Viswanath, K. K. H. De Silva, Y. Morikuni, M. Yoshimura, *Adv. Electron. Mater.* **2021**, *7*, 2001085.
[16] K. L. Kim, W. Lee, S. K. Hwang, S. H. Joo, S. M. Cho, G. Song, S. H. Cho, B. Jeong, I. Hwang, J.-H. Ahn, Y.-J. Yu, T. J. Shin, S. K. Kwak, S. J. Kang, C. Park, *Nano Lett.* **2016**, *16*, 334.
[17] K. Lau, Y. Liu, H. Chen, R. L. Withers, *Adv. Cond. Mat. Phys.* **2013**, *2013*, 435938.
[18] N. Shingne, M. Geuss, B. Hartmann-Azanza, M. Steinhart, T. Thurn-Albrecht, *Polymer* **2013**, *54*, 2737.
[19] I. Stolichnov, P. Maksymovych, E. Mikheev, S. V. Kalinin, A. K. Tagantsev, N. Setter, *Phys. Rev. Lett.* **2012**, *108*, 027603.
[20] R. Gysel, I. Stolichnov, A. K. Tagantsev, N. Setter, P. Mokrý, *J. Appl. Phys.* **2008**, *103*, 084120.
[21] E. Gutiérrez-Fernández, E. Rebollar, J. Cui, T. A. Ezquerra, A. Nogales, *Macromolecules* **2019**, *52*, 7396.
[22] Y. -. Y. Choi, P. Sharma, C. Phatak, D. J. Gosztola, Y. Liu, J. Lee, B. Lee, J. Li, A. Gruverman, S. Ducharme, S. Hong, *ACS Nano* **2015**, *9*, 1809.
[23] P. Sharma, T. J. Reece, S. Ducharme, A. Gruverman, *Nano Lett.* **2011**, *11*, 1970.
[24] P. Sharma, D. Wu, S. Poddar, T. J. Reece, S. Ducharme, A. Gruverman, *J. Appl. Phys.* **2011**, *110*, 052010.
[25] A. Crassous, T. Sluka, A. K. Tagantsev, N. Setter, *Nat. Nanotechn.* **2015**, *10*, 614.
[26] K. Kimura, K. Kobayashi, H. Yamada, T. Horiuchi, K. Ishida, K. Matsushige, et al., *Appl. Phys. Lett.* **2003**, *82*, 4050.
[27] K. Kimura, K. Kobayashi, H. Yamada, K. Matsushige, *Langmuir* **2007**, *23*, 4740.
[28] S. Baskaran, N. Ramachandran, X. He, S. Thiruvannamalai, H. J. Lee, H. Heo, Q. Chen, J. Y. Fu, *Phys. Lett. A* **2011**, *375*, 2082.
[29] R. Roth, M. Koch, J. Schaab, M. Lilienblum, F. Syrowatka, T. Band, T. Thurn-Albrecht, K. Dörr, *New J. Phys.* **2018**, *20*, 103044.
[30] V. S. Bystrov, E. V. Paramonova, I. K. Bdikin, A. V. Bystrova, R. C. Pullar, A. L. Kholkin, *J. Mol. Model* **2013**, *19*, 3591.
[31] S. B. Lang, S. Muensit, *Appl. Phys. A* **2006**, *85*, 125.
[32] R. Ginés, A. Bergamini, R. Christen, M. Motavalli, P. Ermanni, *Smart Mater. Struc.* **2013**, *22*, 075023.
[33] P. Zubko, G. Catalan, A. K. Tagantsev, *Annu. Rev. Mater. Res.* **2013**, *43*, 387.
[34] G. Suresh, S. Jatav, G. Mallikarjunachari, M. S. R Rao, P. Ghosh, D. K. Satapathy, *J. Phys. Chem. B* **2018**, *122*, 8591.
[35] W. Kang, J. E. Huber, *Cell Rep. Phys.l Sci* **2022**, *3*, 100707.
[36] E. Bellet-Amalric, J. F. Legrand, *Eur. Phys. J. B* **1998**, *3*, 225.

[37] I. Katsouras, K. Asadi, M. Li, T. B. Van Driel, K. S. Kjær, D. Zhao, T. Lenz, Y. Gu, P. W. M. Blom, D. Damjanovic, M. M. Nielsen, D. M. De Leeuw, *Nat. Mater.* **2015**, *15*, 78.
[38] Y. Huang, G. Rui, Q. Li, E. Allahyarov, R. Li, M. Fukuto, G.-J. Zhong, J.-Z. Xu, Z.-M. Li, P. L. Taylor, L. Zhu, *Nat. Commun.* **2021**, *12*, 675.
[39] V. V. Kochervinskii, *Crystallogr. Reps.* **2003**, *48*, 649.
[40] G. E. Johnson, L. L. Blyler, N. M. Hulton, *Ferroelectrics* **1980**, *28*, 303.
[41] M. Kumar, D. G. Georgiadou, A. Seitkhan, K. Loganathan, E. Yengel, H. Faber, D. Naphade, A. Basu, T. D. Anthopoulos, K. Asadi, *Adv. Electron. Mater.* **2020**, *6*, 1901091.